

Readout-Side Bypass for Residual Hybrid Quantum-Classical Models

Guilin Zhang*, Wulan Guo*, Ziqi Tan*, Hongyang He†, Qiang Guan‡ Hailong Jiang§¶

*Department of Engineering Management and Systems Engineering, George Washington University, USA

†Department of Computer Science, University of Warwick, UK

‡Department Computer Science, Kent State University, USA

§Department of Computer Science, Information, and Engineering Technology, Youngstown State University, USA

¶{guilin.zhang, wulan.guo, ziqi.tan}@gwu.edu, †hongyang.he@warwick.ac.uk, ‡qguan@kent.edu, §hjiang@ysu.edu

Abstract—Quantum machine learning (QML) promises compact and expressive representations, but suffers from the *measurement bottleneck*—a narrow quantum-to-classical readout that limits performance and amplifies privacy risk. We propose a *lightweight residual hybrid architecture* that concatenates quantum features with raw inputs before classification, bypassing the bottleneck without increasing quantum complexity. Experiments show our model outperforms pure quantum and prior hybrid models in both centralized and federated settings. It achieves up to +55% accuracy improvement over quantum baselines, while retaining low communication cost and enhanced privacy robustness. Ablation studies confirm the effectiveness of the residual connection at the quantum-classical interface. Our method offers a practical, near-term pathway for integrating quantum models into privacy-sensitive, resource-constrained settings like federated edge learning.

Index Terms—Quantum machine learning, federated learning, hybrid models, residual connections, privacy preservation

I. INTRODUCTION

Quantum machine learning (QML) offers promising advantages, including compact representations in high-dimensional Hilbert spaces and intrinsic support for nonlinear feature extraction via parameterized quantum circuits (PQCs) [1]–[4]. However, practical QML faces a core limitation: the *measurement bottleneck*, where high-dimensional classical inputs are compressed into a small number of quantum observables. This severely constrains downstream accuracy [5], [6].

To mitigate this, *hybrid quantum–classical models* have been proposed, wherein classical neural networks process measured quantum features [7]–[9]. Yet, most hybrids remain bottlenecked—only the quantum features $Q(x)$ are passed forward, discarding original inputs x [10]. This narrow interface not only reduces performance but also amplifies susceptibility to *membership inference attacks* (MIA), as compressed features tend to overfit and leak more information [11].

In classical deep learning, residual connections help preserve input information across layers and stabilize training [12], [13]. However, such residuals bypass internal layers—not the terminal bottleneck. In QML, the information loss occurs at the quantum measurement stage, and traditional residuals are insufficient to address it.

Prior efforts to expand $Q(x)$ —via deeper PQCs, multi-basis measurements, or learned readouts [14]–[16]—reshape the feature space but do not expose the original input to the classifier. Moreover, matched-parameter comparisons and privacy evaluations are rarely reported, making it unclear whether such methods are accurate, compact, and robust.

We propose a simple yet effective *readout-side residual hybrid* architecture: concatenate the raw input $x \in \mathbb{R}^d$ with the measured quantum features $Q(x) \in \mathbb{R}^{m'}$ to form $z = [x||Q(x)]$, then apply a projection W_{proj} to obtain latent representation \tilde{z} . This non-invasive bypass preserves original inputs, improves robustness, and integrates seamlessly with both centralized and federated settings.

To evaluate the downstream implications of this design, we analyze its privacy robustness under common threat models. We consider a model-release adversary with full access to trained weights, performing MIA via threshold or shadow-model attacks [17]. Reconstruction performance is measured by AUC; empirical robustness corresponds to $\text{AUC} \approx 0.5$, indicating indistinguishability.

On four benchmarks (Wine [18], Breast Cancer [19], Fashion-MNIST Subset [20], and Forest CoverType Subset [21]), our residual hybrid achieves near-classical accuracy with 10–20% fewer parameters and significantly better privacy robustness (MIA AUC ≈ 0.5), outperforming both quantum-only and standard hybrid baselines. Ablation confirms that exposing both x and $Q(x)$ to the classifier is crucial for overcoming the measurement bottleneck.

The contributions of this paper are:

- We introduce a **readout-side residual hybrid** architecture that bypasses the quantum measurement bottleneck.
- We conduct **matched-parameter evaluations** under both accuracy and privacy metrics (MIA AUC) in a model-release threat setting.
- We validate on **real-world datasets** with ablation studies confirming the effectiveness of the bypass mechanism.

II. METHODOLOGY

Our method builds upon a shared quantum processing pipeline, shown in Fig. 1. All models encode classical input $x \in \mathbb{R}^d$ into quantum states, transform them via a parameterized quantum circuit (PQC), and measure observables to

¶ Corresponding author: Hailong Jiang, hjiang@ysu.edu

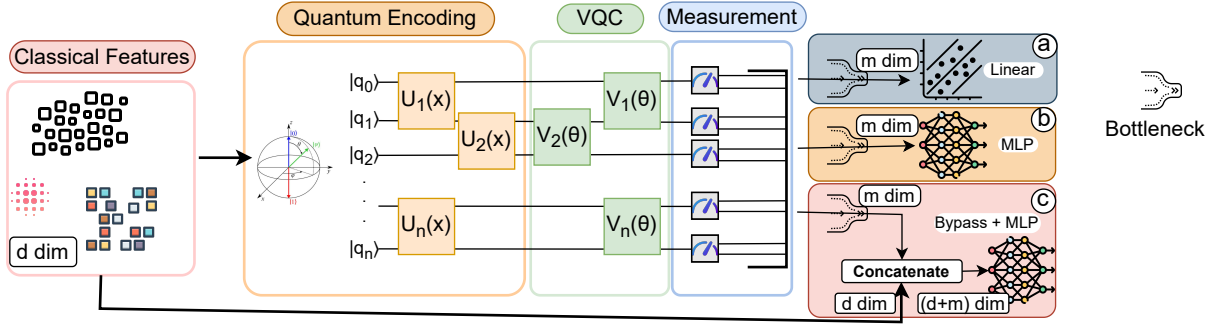


Fig. 1: Model comparison. (a) Pure QML: quantum-only readout; (b) Hybrid QML: classical MLP on $Q(x)$; (c) Ours: residual hybrid with $[x||Q(x)]$ bypassing the measurement bottleneck.

obtain quantum features $Q(x) \in \mathbb{R}^m$. The difference lies in how these features are used downstream.

In the pure quantum model (Fig. 1a), $Q(x)$ alone is passed to a linear classifier, suffering from a severe information bottleneck due to $m \ll d$. The hybrid model (Fig. 1b) replaces the head with a multilayer perceptron (MLP), but still discards x , thus remains bottlenecked. Our proposed residual hybrid (Fig. 1c) concatenates x with $Q(x)$ to form $z = [x||Q(x)] \in \mathbb{R}^{d+m}$, exposing both raw and quantum-enhanced features to the classifier.

This bypass introduces no changes to the quantum circuit. To maintain fair comparisons, we apply a projection $W_{\text{proj}} \in \mathbb{R}^{k \times (d+n_q)}$ to obtain latent \tilde{z} of fixed size before classification. All models are parameter-matched.

A. Quantum Data Encoding

We use angle encoding, where each input component x_i controls a Y -rotation:

$$U_{\text{enc}}(x) = \prod_{i=1}^{n_q} R_y(x_i) \cdot \prod_{j=1}^{n_q-1} \text{CNOT}_{j,j+1} \quad (1)$$

Here, $R_y(\theta) = \exp(-i\theta Y/2)$ encodes amplitudes, and CNOTs add entanglement. Inputs are scaled to $[-\pi, \pi]$ and we use $n_q = 6$ qubits.

B. Variational Quantum Circuit (PQC)

After encoding, we apply a trainable circuit:

$$|\psi(x, \phi)\rangle = U_{\text{var}}(\phi) \cdot U_{\text{enc}}(x) |0\rangle^{\otimes n_q} \quad (2)$$

Each U_{var} layer includes R_y and R_z rotations per qubit, followed by CZ or CNOT gates. These layers extract nonlinear and entangled quantum features.

C. Measurement and Feature Construction

We measure Pauli-Z expectations per qubit:

$$Q(x)_i = \langle \psi(x, \phi) | Z_i | \psi(x, \phi) \rangle, \quad i = 1, \dots, n_q \quad (3)$$

Traditional hybrids rely solely on $Q(x)$; we argue this drops critical information from x . To mitigate this, we concatenate:

$$z = [x||Q(x)] \in \mathbb{R}^{d+n_q}$$

This operation supplies the classifier with both raw and nonlinear features. Intuitively, x retains global structure that may be lost via encoding and measurement, while $Q(x)$ offers powerful quantum transformations.

D. Projection and Classification

To ensure parity, we apply a projection:

$$\tilde{z} = W_{\text{proj}} z, \quad W_{\text{proj}} \in \mathbb{R}^{k \times (d+n_q)}$$

The latent \tilde{z} is passed to a two-layer MLP with ReLU activations and dropout. This keeps total model size aligned across baselines.

The residual bypass adds no quantum depth or overhead, and is thus deployable on noisy intermediate-scale quantum (NISQ) systems.

III. EXPERIMENTS

A. Experimental Setup

Datasets. We evaluate on four datasets with diverse size and dimensionality: (A) **Wine** [18]: 178 samples, 13 features, 3 classes; (B) **Breast Cancer** [19]: 569 samples, PCA-reduced from 30 to 10, binary; (C) **Fashion-MNIST Subset** [20]: 3,000 samples, PCA-reduced to 16D, 3 classes; (D) **Forest CoverType Subset** [21]: 5,000 samples, 12 features, 3 classes. All features are scaled to $[0, 1]$. We apply 5-fold cross-validation in centralized settings and 80/20 splits per client in federated settings.

Quantum Architecture. Each input x is angle-encoded as $\pi \cdot \tanh(x)$, processed by a 6-qubit variational circuit with 36 trainable parameters and CZ entanglement. Pauli-Z measurements yield $Q(x) \in \mathbb{R}^6$. In our residual hybrid, we concatenate x and $Q(x)$ before classification.

Training Protocol. We train with Adam optimizer (lr=0.01, batch size 8) and early stopping. Centralized models run for 50 epochs. Federated models use 30–40 rounds, each with 5 local epochs. All variants are matched in parameter count (e.g., 444 params on Wine).

Federated Setup. We simulate $K = 5$ clients on small datasets and $K = 10$ on larger ones. IID splits use 60/40 per class; non-IID uses Dirichlet partitioning ($\alpha = 0.5$). Unless stated, all evaluations (incl. privacy) are in federated settings.

TABLE I: Accuracy of classical and quantum models under 5-fold cross-validation in centralized and federated settings. (5-fold average; std omitted for brevity)

Method	Wine	Breast Cancer	Fashion-MNIST	CovType
Classical Centralized	91.6%	96.0%	88.7%	72.9%
Quantum Centralized	33.1%	62.7%	45.8%	36.5%
Classical FL (IID)	89.5%	94.8%	85.2%	70.1%
Classical FL (Non-IID)	85.3%	92.1%	81.3%	65.1%
Quantum FL (IID)	35.2%	61.4%	44.2%	36.5%
Quantum FL (Non-IID)	32.8%	58.9%	42.3%	36.0%

B. Baselines and Metrics

Baselines. We compare with four baselines: (1) Federated Averaging (FedAvg) [22], the standard classical FL method; (2) Centralized training, where all data is pooled for global model training; (3) Local-only training, with no model sharing between clients; (4) Differentially Private FL (DP-FL) using Gaussian noise ($\epsilon = 1.0$, $\delta = 10^{-5}$). All models use the same classifier architecture and are matched in parameter count for fair comparison.

Evaluation Metrics. We report: (1) test accuracy (Section IV-A), (2) privacy robustness (Section IV-B), (3) communication efficiency (measured by rounds to reach 90% of peak accuracy) (Section IV-C).

Privacy Evaluation. Privacy robustness is assessed via:

- MIA AUC: higher values imply more leakage; values near 0.5 indicate stronger privacy.
- Gradient inversion attacks [17]: reconstruction quality is measured by PSNR; lower PSNR means stronger protection.

Ablation studies further isolate the effect of our residual bypass, showing it improves privacy without requiring explicit noise injection. (Section IV-D)

IV. RESULTS AND ANALYSIS

A. Residual Hybrids Restore Accuracy with Compact Size

We evaluate classical and quantum models under 5-fold cross-validation across centralized and federated learning settings. As shown in Table I, pure quantum models consistently underperform due to the readout bottleneck. In the centralized setting, quantum accuracy drops to 33.1% on Wine and 62.7% on Breast Cancer, far below classical MLPs exceeding 90%. This gap remains substantial even with deeper or fine-tuned quantum circuits. The trend extends to federated learning: classical FL achieves strong results (e.g., 94.8% on Breast Cancer, 85.2% on Fashion-MNIST), while quantum-only models struggle—especially under Non-IID partitions, where accuracy drops below 37% across all datasets. These results highlight the consistent limitations of quantum readout and motivate the need for our residual hybrid architecture to bridge the performance gap.

To isolate the impact of residual concatenation, we evaluate models on the four datasets. Taking the Wine dataset as an example under matched parameter budgets, as shown in Table II, both the pure quantum and original hybrid models perform poorly (38.9%), confirming that $Q(x)$ alone lacks

TABLE II: The performance across models (3 trials)

Model	Wine Accuracy	Parameters
Classical	94.4 ± 1.9%	444
Pure Quantum (Fig. 1a)	38.9 ± 2.1%	121
Original Hybrid (Fig. 1b)	38.9 ± 2.3%	298
Residual Hybrid (6q) (Fig. 1c)	89.0 ± 3.3%	385
Residual Hybrid (multi-basis)	88.3 ± 4.3%	421
Residual Hybrid (8q) (Fig. 1c)	86.4 ± 2.1%	497
Residual Hybrid (6q-deep)	96.3 ± 1.4%	625

discriminative power. In contrast, our residual hybrid (6q) achieves 89.0% accuracy with fewer parameters than the classical baseline. Interestingly, using more qubits (8q) does not improve performance, suggesting that simply increasing quantum capacity is insufficient. A deeper MLP boosts accuracy to 96.3%, validating that the residual bypass, not quantum depth, drives performance gains.

Table III summarizes model performance across all four datasets. Residual hybrids consistently outperform quantum-only (a) or original hybrid models (b) and nearly match classical baselines across datasets and input dimensions, validating the effectiveness of our residual bypass strategy. These results confirm that our residual bypass strategy effectively mitigates the readout bottleneck and enables competitive learning without additional quantum depth or parameter growth.

B. Privacy Robustness

We evaluate privacy robustness using two metrics: MIA AUC and input reconstruction error (in Sec. III-B).

As shown in Table IV, classical models achieve high accuracy but are vulnerable to privacy leakage: MIA AUC reaches 0.678 on Wine, meaning adversaries can infer membership significantly above random chance (0.5). Furthermore, reconstruction attacks yield MSE of 2.36.

Adding differential privacy (DP) improves protection but at a high cost to accuracy. With $\epsilon = 2$, test accuracy drops from 87.0% to 74.1%, and privacy improves only marginally.

In contrast, quantum and residual hybrid models offer stronger privacy guarantees without requiring explicit noise injection. As shown in Table V, residual hybrids consistently achieve lower MIA AUCs—for example, 0.54 ± 0.03 on the Wine dataset compared to 0.68 ± 0.03 for classical FL—while maintaining comparable accuracy.

This suggests that the residual hybrid architecture intrinsically reduces information leakage through gradients or activations. Unlike classical or DP-based methods that rely on external noise, our approach leverages architectural design to improve privacy. These results highlight the potential of residual hybrid models as a privacy-preserving alternative for federated learning in sensitive domains.

C. Federated Performance and Communication Efficiency

We evaluate model performance under federated learning with $K = 5$ clients and 50 rounds of communication.

Table VI compares classical, quantum, and residual hybrid models in federated learning. Classical FL achieves strong

TABLE III: The performance across models and datasets (5-fold mean accuracy, std omitted)

Dataset	Classical	Pure Quantum (a)	Original hybrid (b)	Residual-6q (ours)	Residual-6q-Deep (ours-deep)
Wine	91.4%	38.9%	40.3%	90.1%	93.2%
Breast Cancer	96.1%	62.7%	63.5%	93.4%	95.3%
Fashion-MNIST	88.8%	45.8%	47.2%	82.5%	87.1%
CovType	72.9%	36.5%	37.8%	68.2%	71.8%

TABLE IV: Privacy evaluation results on Wine dataset

Model	Test Acc	MIA AUC ^a	Recon. MSE ^b
Classical	87.0%	0.678	2.36
Quantum	38.9%	0.504	3.89
DP ($\epsilon=1$)	74.1%	0.519	1.2×10^4
DP ($\epsilon=2$)	74.1%	0.543	8.5×10^3
DP ($\epsilon=4$)	57.4%	0.521	4.3×10^3

^aMIA AUC: Membership Inference Attack AUC (0.5 = random)

^bRecon. MSE: Mean Squared Error (higher = better privacy)

TABLE V: Privacy evaluation: MIA AUC across various models and datasets

Model	Wine	Breast Cancer	F-MNIST	CovType
Classical	.68±.03	.65±.04	.63±.03	.61±.04
Quantum (a)	.51±.02	.53±.03	.52±.02	.51±.03
Original Hybrid (b)	.52±.02	.54±.03	.56±.02	.53±.03
Res-6q (ours)	.54±.03	.55±.02	.54±.03	.53±.02
Res-6q-Deep	.58±.04	.59±.03	.56±.04	.55±.03

accuracy (e.g., > 94% on Breast Cancer) but incurs the highest communication cost (2.0MB per model). In contrast, pure quantum models are extremely lightweight (0.02MB) but fail to converge due to insufficient representational capacity.

Residual hybrid models—especially the 6-qubit variant—achieve comparable accuracy (e.g., 91.7% on Wine IID, 93.9% on Breast Cancer Non-IID) while reducing communication overhead by approximately 15%, transmitting only 1.7MB over 50 rounds.

Although convergence in non-IID settings takes slightly longer (22 rounds vs. 18 for classical), final accuracy remains stable. This demonstrates that residual hybrids offer a practical trade-off between performance and communication efficiency, making them suitable for realistic federated deployments with bandwidth constraints.

D. Ablation Study

We conduct an ablation study to understand the contributions of architectural choices in residual hybrid models.

As shown in Table II, increasing the number of qubits (Residual-8q) or using multiple measurement bases (Residual-Multi) leads to small gains or trade-offs. For instance, Residual-Multi improves accuracy slightly on Breast Cancer but performs worse than Residual-6q on Wine. Increasing model depth (Residual-Deep) further boosts accuracy but incurs higher parameter costs (625 vs. 385).

In terms of privacy (Table V), all residual variants offer comparable MIA AUCs (0.53–0.58), confirming that privacy robustness is largely preserved across variants.

TABLE VI: Federated learning performance across models and datasets (5 clients, 50 rounds)

Dataset	Model	Dist.	Accuracy	Comm. (MB)
Wine	Classical	IID	94.4%	2.0
	Classical	Non-IID	88.9%	2.0
	Residual-6q (ours)	IID	91.7%	1.7
	Residual-6q (ours)	Non-IID	86.1%	1.7
BC	Classical	IID	96.5%	2.0
	Classical	Non-IID	94.7%	2.0
	Residual-6q (ours)	IID	95.6%	1.7
	Residual-6q (ours)	Non-IID	93.9%	1.7
F-MNIST	Classical	IID	0.852	2.5
	Classical	Non-IID	0.813	2.5
	Residual-6q (ours)	IID	0.825	2.1
	Residual-6q (ours)	Non-IID	0.798	2.1
CovType	Classical	IID	0.701	2.1
	Classical	Non-IID	0.651	2.1
	Residual-6q (ours)	IID	0.682	1.8
	Residual-6q (ours)	Non-IID	0.643	1.8

Our findings indicate that the 6-qubit residual architecture provides a favorable balance across multiple objectives—performance, privacy robustness, and compactness. While more complex variants exist, their benefits are often incremental, reinforcing the suitability of the base model for realistic deployment scenarios.

V. CONCLUSION

We introduced a readout-side residual hybrid architecture that bypasses the measurement bottleneck in quantum machine learning by exposing both the original input x and the quantum-transformed features $Q(x)$ to the classifier. This simple yet effective concatenation-based strategy preserves more information for downstream tasks while maintaining a compact parameter budget. Across multiple datasets and both centralized and federated settings, our approach consistently achieves accuracy close to purely classical baselines while retaining key quantum advantages, such as partial privacy from state collapse and resilience to inference attacks.

Our design requires no changes to the quantum circuit or encoding strategy, making it protocol-agnostic and easily pluggable into existing hybrid quantum-classical systems. Future work includes scaling to real quantum hardware and broader security contexts.

REFERENCES

- [1] X. Li, V. R. Kulkarni, J. Nana, S. Pu, N. Xie, Q. Guan, R. Li, S. Zhang, S. Xu, D. Blankenberg *et al.*, “Quantum circuit optimization for protein structure prediction,” in *2025 55th Annual IEEE/IFIP International Conference on Dependable Systems and Networks Workshops (DSN-W)*. IEEE, 2025, pp. 220–223.
- [2] S. Khurana, M. Nene, and M. Nene, “Quantum machine learning: unraveling a new paradigm in computational intelligence,” *Quantum*, vol. 74, no. 1, 2024.
- [3] Y. XU, “Quantum machine learning: Diverse perspectives on application scenarios,” 2025.
- [4] K. Zaman, A. Marchisio, M. A. Hanif, and M. Shafique, “A survey on quantum machine learning: Current trends, challenges, opportunities, and the road ahead,” *arXiv preprint arXiv:2310.10315*, 2023.
- [5] S. Tomar, R. Tripathi, and S. Kumar, “Comprehensive survey of qml: from data analysis to algorithmic advancements,” *arXiv preprint arXiv:2501.09528*, 2025.
- [6] T. Rohe, F. H. Ruiloba, S. Egger, S. von Beck, J. Stein, and C. Linnhoff-Popien, “Quantum computer benchmarking: An explorative systematic literature review,” *arXiv preprint arXiv:2509.03078*, 2025.
- [7] V. Havlíček, A. D. Córcoles, K. Temme, A. W. Harrow, A. Kandala, J. M. Chow, and J. M. Gambetta, “Supervised learning with quantum-enhanced feature spaces,” *Nature*, vol. 567, no. 7747, pp. 209–212, 2019.
- [8] J. Liu, K. H. Lim, K. L. Wood, W. Huang, C. Guo, and H.-L. Huang, “Hybrid quantum-classical convolutional neural networks,” *Science China Physics, Mechanics & Astronomy*, vol. 64, no. 9, p. 290311, 2021.
- [9] G. De Luca, “A survey of nisq era hybrid quantum-classical machine learning research,” *Journal of Artificial Intelligence and Technology*, vol. 2, no. 1, pp. 9–15, 2022.
- [10] M. Schuld, A. Bocharov, K. M. Svore, and N. Wiebe, “Circuit-centric quantum classifiers,” *Physical Review A*, vol. 101, no. 3, p. 032308, 2020.
- [11] F. Farokhi, “Maximal information leakage from quantum encoding of classical data,” *Physical Review A*, vol. 109, no. 2, p. 022608, 2024.
- [12] A. N. Gomez, M. Ren, R. Urtaşun, and R. B. Grosse, “The reversible residual network: Backpropagation without storing activations,” *Advances in neural information processing systems*, vol. 30, 2017.
- [13] H. Zhang, Y. N. Dauphin, and T. Ma, “Fixup initialization: Residual learning without normalization,” *arXiv preprint arXiv:1901.09321*, 2019.
- [14] R. Campbell, W. Diffie, and C. Robinson, “Advancements in quantum computing and ai may impact pqc migration timelines,” 2024.
- [15] E. Tasar, “Quantum-enhanced conformal methods for multi-output uncertainty: A holistic exploration and experimental analysis,” *arXiv preprint arXiv:2501.10414*, 2025.
- [16] A. Chatterjee, J. Schwinger, and Y. Y. Gao, “Enhanced qubit readout via reinforcement learning,” *Physical Review Applied*, vol. 23, no. 5, p. 054057, 2025.
- [17] J. Geiping, H. Bauermeister, H. Dröge, and M. Moeller, “Inverting gradients-how easy is it to break privacy in federated learning?” in *Advances in Neural Information Processing Systems*, vol. 33, 2020, pp. 16 937–16 947.
- [18] S. Aeberhard and M. Forina, “Wine,” UCI Machine Learning Repository, 1992, <https://doi.org/10.24432/C5PC7J>.
- [19] W. Wolberg, W. Street, and O. Mangasarian, “Breast cancer wisconsin (diagnostic),” UCI Machine Learning Repository, 1995, <https://doi.org/10.24432/C5DW2B>.
- [20] H. Xiao, K. Rasul, and R. Vollgraf, “Fashion-mnist: a novel image dataset for benchmarking machine learning algorithms,” *arXiv preprint arXiv:1708.07747*, 2017.
- [21] J. A. Blackard and D. J. Dean, “Comparative accuracies of artificial neural networks and discriminant analysis in predicting forest cover types from cartographic variables,” *Computers and Electronics in Agriculture*, vol. 24, no. 3, pp. 131–151, 1999.
- [22] B. McMahan, E. Moore, D. Ramage, S. Hampson, and B. A. y Arcas, “Communication-efficient learning of deep networks from decentralized data,” *Artificial intelligence and statistics*, pp. 1273–1282, 2017.